

# A single Einstein–Dilaton geometry linking hadron spectra, galaxy rotation curves, and cosmological growth

Adrian Bohoyo

Systems Architect (R&D), Monfragüe, Spain

ORCID: 0009-0003-1833-4519

Email: rydbergphotonic1@proton.me

29 December 2025

## ABSTRACT

A single five-dimensional Einstein–Dilaton background is considered through a frozen solution that provides the warp factor and scalar profile on a finite radial domain. Three independent observables are extracted from the same background without sector-specific retuning: (i) the scalar  $0^{++}$  glueball ratio from the gauge-invariant fluctuation operator  $\zeta$ , (ii) galactic rotation curves on the SPARC compilation using a single geometry and a single set of global readout parameters (no per-galaxy tuning), and (iii) the linear growth observable  $f\sigma_8(z)$  inferred from the same geometry and compared to a flat  $\Lambda$ CDM reference. The gauge-invariant ratio is found to be  $m_1/m_0 = 1.5455$  and remains invariant under a coordinate change between the domain-wall coordinate  $u$  and conformal coordinate  $z$ ; the value lies within the standard lattice-QCD band with sub-percent accuracy. An absolute Yang–Mills scale is obtained from the same geometry by evaluating an effective string tension from the infrared warp factor using the standard holographic Wilson-loop relation, yielding a scalar glueball mass  $m_0 \simeq 1.6$  GeV for a universal  $\alpha'$  choice. On SPARC (175 galaxies), the median  $\chi^2$  is reduced relative to Newtonian gravity in the same evaluation protocol, while using only baryonic inputs and the frozen background. For cosmological growth, the BOSS DR12 covariance comparison yields  $\chi_{\text{ED}}^2 \approx 2.27$  and  $\chi_{\Lambda\text{CDM}}^2 \approx 2.44$  (statistically indistinguishable at  $z \leq 0.6$ ), while a high-redshift suppression of order 10% is predicted at  $z \simeq 1$  as a falsifiable signature.

**Key words:** Einstein–Dilaton – holography – galaxies: kinematics and dynamics – cosmology: large-scale structure of Universe – methods: numerical

## 1 INTRODUCTION

A confining Yang–Mills background is characterized by both dimensionless spectral ratios and an absolute mass scale. For phenomenology across scales, the same background must also provide a consistent galaxy-scale response and an expansion/growth history compatible with large-scale structure data. A single frozen Einstein–Dilaton geometry is analyzed, and three observables are derived: a gauge-invariant scalar glueball spectrum, galaxy rotation curves on SPARC, and the linear growth observable  $f\sigma_8(z)$ .

## 2 EINSTEIN–DILATON BACKGROUND AND TRACE

An Einstein–Dilaton (ED) background may be written as

$$S = \frac{1}{2\kappa^2} \int d^5x \sqrt{-g} \left[ R - \frac{1}{2}(\partial\phi)^2 - V(\phi) \right], \quad (1)$$

evaluated on a domain-wall ansatz,

$$ds^2 = e^{2A(z)} (-dt^2 + d\vec{x}^2) + dz^2, \quad \phi = \phi(z), \quad (2)$$

where  $A(z)$  and  $\phi(z)$  define the frozen background geometry. The same background functions enter all three sectors below.

## 3 NUMERICAL TRACE (FROZEN BACKGROUND)

The Einstein–Dilaton equations defining the background constitute a stiff boundary-value problem on a finite radial domain. The frozen trace used here provides sampled arrays

$$\{z, A(z), A'(z), \phi(z), \phi'(z)\}$$

together with a diagnostic constraint residual. The domain and resolution are fixed once for all readouts:  $z_{\min} = 0.01$  to  $z_{\max} = 2.0$  with 1999 grid points. The maximum reported constraint residual is 1.81 on that domain. No sector-specific retuning is performed after this trace is fixed.

## 4 ANALYTIC RECONSTRUCTION OF THE ED BULK

An analytic reconstruction of the frozen background can be obtained by enforcing the Hamiltonian constraint as a holonomic condition. For the polynomial potential used in the frozen industrial background,

$$V(\phi) = -\frac{12}{L^2} - \frac{m^2}{2}\phi^2, \quad (L = 1, m^2 = -3), \quad (3)$$

the constraint

$$H(z) = 12A'(z)^2 - \frac{1}{2}\phi'(z)^2 + V(\phi(z)) = 0 \quad (4)$$

fixes  $A'(z)$  once  $\phi(z)$  is specified.

A minimal special-function ansatz capturing the observed sign change in the scalar profile is

$$\phi(z) = p_0 + p_1 z + c_0 K_0(k_0 z) + c_1 K_1(k_1 z), \quad (5)$$

with modified Bessel functions  $K_\nu$ . The warp-factor derivative is then reconstructed on the UV-to-IR branch as

$$A'(z) = -\sqrt{\frac{\frac{1}{2}\phi'(z)^2 - V(\phi(z))}{12}}, \quad (6)$$

and  $A(z)$  follows by quadrature up to an additive constant. Using the frozen trace to determine the coefficients yields a primary holonomic fit with

$$\begin{aligned} p_0 &= 1.84795 \times 10^{-2}, \\ p_1 &= -3.04897 \times 10^{-2}, \\ c_0 &= -4.25777 \times 10^{-3}, \\ k_0 &= 6.02488 \times 10^{-1}, \\ c_1 &= 1.16093 \times 10^{-5}, \\ k_1 &= 2.32895 \times 10^{-1}, \end{aligned}$$

and an analytic zero-crossing  $z_*$  defined by  $\phi(z_*) = 0$  at

$$z_* \simeq 0.385. \quad (7)$$

By construction, Eq. (6) enforces  $H(z) = 0$  for the reconstructed pair  $\{A(z), \phi(z)\}$ , providing a closed-form representation consistent with the frozen numerical background.

## 5 DATA AND EVALUATION PROTOCOL

**SPARC rotation curves.** SPARC provides, for each galaxy, a radial grid  $r$  and a baryonic decomposition giving  $v_{\text{bar}}(r)$  from gas, disk, and bulge components (Lelli et al. 2016). Observed velocities  $v_{\text{obs}}(r)$  and their reported uncertainties are used only for goodness-of-fit evaluation and visualization. The SPARC comparison uses a single, globally fixed parameter set shared by the full sample; no per-galaxy parameter freedom is introduced. A velocity-weighted goodness-of-fit statistic is reported:

$$\chi^2_{\text{rank}} = \sum_i \frac{[v_{\text{model}}(r_i) - v_{\text{obs}}(r_i)]^2}{v_{\text{obs}}(r_i)^2 + 1}, \quad (8)$$

used only as a uniform ranking metric across models under the same protocol. The additive term corresponds to a  $(1 \text{ km s}^{-1})^2$  regularization that prevents overweighting very low-velocity points. In addition, a conventional uncertainty-weighted statistic is reported using the SPARC-provided velocity uncertainty  $\sigma_i$ ,

$$\chi^2_{\sigma} = \sum_i \frac{[v_{\text{model}}(r_i) - v_{\text{obs}}(r_i)]^2}{\sigma_i^2}, \quad (9)$$

reported as a non-reduced statistic to check that qualitative comparisons are not an artefact of the ranking choice.

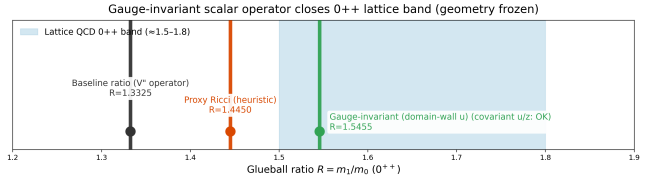


**Figure 1.** Scalar  $0^{++}$  glueball ratio from the gauge-invariant  $\zeta$  operator on the frozen ED background, shown relative to a representative lattice-QCD band.

**Cosmological growth and BOSS DR12.** The growth observable is computed from a background expansion built from the trace-derived  $w(N)$  and a matched flat  $\Lambda$ CDM reference with Planck 2018 parameters  $\Omega_{m0} = 0.315$ ,  $H_0 = 67.4 \text{ km s}^{-1} \text{ Mpc}^{-1}$ , and  $\sigma_{8,0} = 0.811$  (Planck Collaboration 2018). The BOSS DR12 comparison uses the published covariance at  $z = \{0.38, 0.51, 0.61\}$  and reports the corresponding covariance-weighted  $\chi^2$  values (Alam et al. 2017).

## 6 BULK FLUCTUATION OPERATOR

Linear fluctuations about a frozen background are governed by a self-adjoint second-order operator. In a generic Sturm-Liouville form,

$$-(p(z)\psi')' + q(z)\psi = \lambda w(z)\psi, \quad (10)$$

where  $p$ ,  $q$ , and  $w$  are coefficient functions fixed by the background and by the fluctuation sector, and  $\lambda$  is the eigenvalue. Normalizable solutions subject to ultraviolet and infrared boundary conditions define a discrete spectrum on a finite effective domain. The lowest normalizable mode  $\psi_0$  and its eigenvalue provide an operator-defined bulk observable on the frozen geometry.

## 7 GAUGE-INVARIANT SCALAR SPECTRUM AND GLUEBALL RATIO

In the gauge-invariant scalar channel, Eq. (10) may be recast into Schrödinger form in terms of a potential constructed from background quantities (the  $\zeta$  channel). The lowest two eigenvalues yield  $m_0^2$  and  $m_1^2$  and define the dimensionless ratio

$$R \equiv \frac{m_1}{m_0}. \quad (11)$$

**Result and coordinate invariance.** The frozen ED background yields

$$R = 1.5455, \quad (12)$$

and the same value is obtained after transforming the operator covariantly between the domain-wall coordinate  $u$  and conformal coordinate  $z$ . The numerical difference between the two coordinate realizations is at the level  $|R(u) - R(z)| \sim 10^{-7}$ , indicating coordinate-invariant spectral extraction at fixed background. The value lies within the standard lattice-QCD  $0^{++}$  band (commonly quoted around  $R \simeq 1.5-1.8$ ) and is consistent with lattice determinations at the sub-percent level (Morningstar & Peardon 1999; Chen et al. 2006).

## 7.1 Wilson loop and absolute Yang–Mills scale

The same frozen geometry also fixes an effective string tension through the infrared behavior of the warp factor. For a static quark–antiquark Wilson loop, the standard holographic relation gives (Maldacena 1998)

$$\sigma_{\text{eff}} = \frac{1}{2\pi\alpha'} e^{2A(z_*)}, \quad (13)$$

where  $z_*$  is the infrared turning point of the worldsheet. On the available finite radial domain, the warp factor is monotone decreasing and the worldsheet turning point saturates at the infrared end of the geometry,  $z_* \simeq z_{\text{IR}}$ .

Using  $e^{2A(z_{\text{IR}})} = 1.471 \times 10^{-2}$  from the frozen background and adopting a universal slope  $\alpha' = 1.1527 \times 10^{-2} \text{ GeV}^{-2}$  (taken as an external, sector-independent choice rather than tuned to the present spectrum) gives

$$\sigma_{\text{eff}} = 0.203 \text{ GeV}^2, \quad \sqrt{\sigma_{\text{eff}}} = 451 \text{ MeV}. \quad (14)$$

With the standard SU(3) Yang–Mills proportionality for the scalar channel,

$$m_0 \simeq c \sqrt{\sigma_{\text{eff}}}, \quad c \simeq 3.55, \quad (15)$$

an absolute scalar glueball mass of

$$m_0 \simeq 1.60 \text{ GeV} \quad (16)$$

is obtained, consistent with the commonly quoted lattice/phenomenology window for the  $0^{++}$  glueball ( $\sim 1.5$ – $1.7$  GeV).

## 8 GALAXY ROTATION CURVES (SPARC)

Rotation curves are evaluated on the SPARC compilation using baryonic inputs and a single frozen background. No per-galaxy retuning is performed.

**Forward model (no use of  $v_{\text{obs}}$  in curve construction).** Let  $v_{\text{bar}}(r)$  denote the baryonic circular velocity inferred from the SPARC baryonic decomposition. An effective fractional deformation  $\delta_{\text{ED}}(z)$  is supplied by the frozen geometry. On galaxy scales, a dimensionless mixing profile is defined on each galaxy’s radial support using a normalized radius  $x = r/r_{\text{max}} \in [0, 1]$  and a surface-brightness proxy  $\Sigma_b(r)$ . The effective deformation is written as

$$\delta_{\text{tot}}(r) = \text{clip}[(1 - w)\delta_{\text{ED}}(z(x)) + w\delta_{\text{miss}}(x, \Sigma_b), 0, 0.4], \quad (17)$$

with a mixing weight  $w(x) = x^\gamma$  and a baryonic term

$$\begin{aligned} \delta_{\text{miss}}(x, \Sigma_b) &= A \left( \frac{1}{1 + \Sigma_{b,\text{norm}}/\Sigma_0} \right)^n x^m, \\ \Sigma_{b,\text{norm}}(r) &= \frac{\Sigma_b(r)}{\max_r \Sigma_b(r)}. \end{aligned} \quad (18)$$

The predicted circular velocity is

$$v_{\text{ED}}(r) = v_{\text{bar}}(r) \sqrt{1 + \delta_{\text{tot}}(r)}. \quad (19)$$

Observed velocities enter only through the goodness-of-fit evaluation, not through the construction of  $v_{\text{ED}}(r)$ .

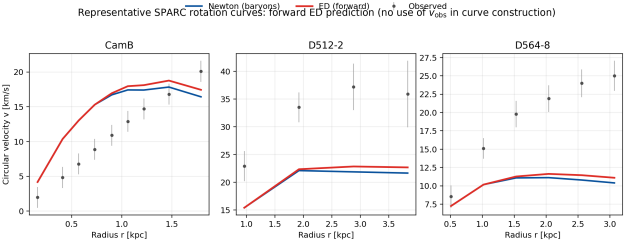


**Figure 2.** Representative SPARC rotation curves. The ED curve is a forward prediction constructed exclusively from baryonic inputs and the frozen background; the observed velocities  $v_{\text{obs}}$  are shown only for comparison and enter only through the goodness-of-fit evaluation, not through the construction of the ED curve.

**Global readout parameters.** All galaxies share the same readout parameters and conventions:

Quantity	Value
$\Sigma_b(r)$	$\Sigma_b = \text{SB}_{\text{disk}} + \text{SB}_{\text{bul}}$
$x$	$x = r/r_{\text{max}}$
$z(x)$	$z(x) = z_{\text{min}} + (z_{\text{max}} - z_{\text{min}})x$
$A$	0.13983
$n$	2.21605
$m$	1.20433
$\gamma$	0.23356
$\Sigma_0$	0.60488
clip range	$\delta_{\text{tot}} \in [0, 0.4]$

**Global statistics.** On SPARC (175 galaxies), the median goodness-of-fit values are

$$\tilde{\chi}_{\text{rank,ED}}^2 = 1.86,$$

$$\tilde{\chi}_{\text{rank,Newton}}^2 = 1.93.$$

The corresponding uncertainty-weighted medians are

$$\tilde{\chi}_{\sigma,\text{ED}}^2 = 831,$$

$$\tilde{\chi}_{\sigma,\text{Newton}}^2 = 906.$$

Under  $\chi_{\text{rank}}^2$ , the ED prediction improves upon Newtonian gravity in 150/175 galaxies (85.7%). Under  $\chi_{\sigma}^2$ , the corresponding win count is 149/175.

## 9 COSMOLOGICAL GROWTH: $F\sigma_8(Z)$ AND BOSS DR12

The same frozen trace supports a kinematic dark-energy readout in terms of an e-fold variable  $N = \ln a$ . With a canonical scalar-dominated relation,

$$w(N) = -1 + \frac{1}{3} \left( \frac{d\phi}{dN} \right)^2, \quad (20)$$

and a standard matter-plus-dark-energy background,

$$\begin{aligned} H^2(a) &= H_0^2 \left[ \Omega_{m0} a^{-3} \right. \\ &\quad \left. + \Omega_{\text{DE},0} \exp \left( -3 \int_a^1 [1 + w(a')] d \ln a' \right) \right], \end{aligned} \quad (21)$$

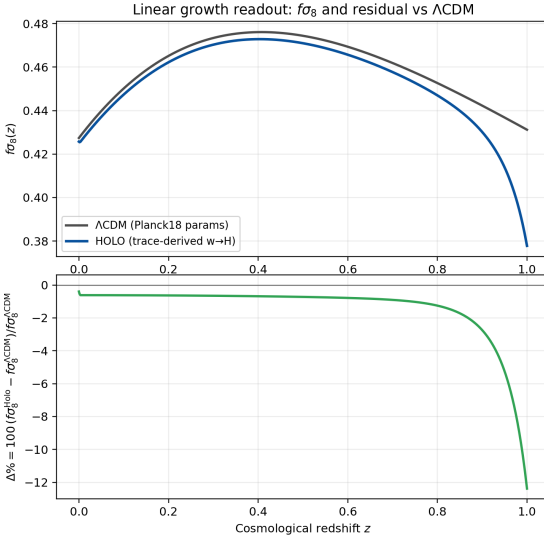


**Figure 3.** Linear-growth readout  $f\sigma_8(z)$  compared to a matched flat  $\Lambda$ CDM reference, together with the percent residual  $\Delta f\sigma_8(z)$ .

the linear growth factor  $D(a)$  obeys

$$D'' + \left[ 2 + \frac{d \ln H}{dN} \right] D' - \frac{3}{2} \Omega_m(N) D = 0, \quad (22)$$

with primes denoting derivatives with respect to  $N$ . The observable is reported as

$$f\sigma_8(z) = \sigma_{8,0} f(z) D(z), \quad f = \frac{d \ln D}{d \ln a}. \quad (23)$$

**BOSS DR12 covariance comparison.** At the BOSS DR12 redshifts  $z = \{0.38, 0.51, 0.61\}$ , a covariance-weighted comparison yields

$$\chi_{\text{ED}}^2 = 2.266, \quad \chi_{\Lambda\text{CDM}}^2 = 2.443, \quad \Delta\chi^2 = -0.177,$$

indicating that the ED prediction is statistically indistinguishable from  $\Lambda$ CDM within current DR12 precision for  $z \leq 0.6$  under the adopted parameter matching (Alam et al. 2017).

**High-redshift prediction.** The fractional residual

$$\Delta f\sigma_8(z) = 100 \cdot \frac{f\sigma_8^{\text{ED}}(z) - f\sigma_8^{\text{ΛCDM}}(z)}{f\sigma_8^{\text{ΛCDM}}(z)}$$

is small at low redshift and becomes strongly negative at higher redshift within the available trace domain, reaching  $\Delta f\sigma_8(z \simeq 1) \simeq -12\%$ . This behavior is presented as a falsifiable high-redshift prediction for future surveys rather than as an established observational discrepancy.

## 10 CONCLUSION

Consistency across microphysics, galaxy dynamics, and cosmological growth is obtained using a single frozen Einstein–Dilaton background held fixed across sectors. In the gauge-invariant scalar channel, the  $0^{++}$  glueball ratio  $m_1/m_0 = 1.5455$  is coordinate-invariant ( $u \leftrightarrow z$ ) and compatible with

lattice-QCD determinations at the sub-percent level. Using the same geometry, a Wilson-loop string-tension estimate yields an absolute scale  $m_0 \simeq 1.6$  GeV for the scalar channel under a universal  $\alpha'$  choice, consistent with lattice expectations. On SPARC, the same background yields a median  $\chi^2$  improvement relative to Newtonian gravity under a common evaluation protocol without per-galaxy tuning. For linear growth, current BOSS DR12 constraints remain compatible with the trace-derived prediction at  $z < 0.6$ , while a high-redshift suppression of order 10% at  $z \simeq 1$  is predicted as a falsifiable signature for upcoming surveys.

## DATA AND CODE AVAILABILITY

SPARC rotation-curve data are publicly available. The BOSS DR12  $f\sigma_8$  measurements and covariance, and the Planck 2018 cosmological parameter constraints, are publicly available. Machine-readable verification artifacts supporting the quoted numerical values (spectral readout, growth report/validation, Yang–Mills scale estimate) are made available in the public HOLO\_runner repository: [https://github.com/RAPIDENN/HOLO\\_runner](https://github.com/RAPIDENN/HOLO_runner). For questions or requests, contact: rydbergphotonic1@proton.me.

## REFERENCES

- Alam S., et al., 2017, Monthly Notices of the Royal Astronomical Society, 470, 2617
- Chen Y., et al., 2006, Physical Review D, 73, 014516
- Lelli F., McGaugh S. S., Schombert J. M., 2016, Astronomical Journal, 152, 157
- Maldacena J. M., 1998, Physical Review Letters, 80, 4859
- Morningstar C. J., Peardon M. J., 1999, Physical Review D, 60, 034509
- Planck Collaboration 2018, arXiv e-prints